Velocity measurements in developing narrow open-channel flows with high free-stream turbulence: Acoustic Doppler Velocimetry (ADV) vs Laser Doppler Anemometry (LDA)

Marie Rastello, Matthew R Klema, Alex B Carpenter, Amrapalli Garanaik, S Karan Venayagamoorthy, Timothy K Gates, J L Marié

Velocity measurements in developing narrow open-channel flows with high free-stream turbulence: Acoustic Doppler Velocimetry (ADV) vs Laser Doppler Anemometry (LDA)

Marie Rastello[1,2], Matthew R. Klema[2,3], Alex B. Carpenter[2], Amrapalli Garanaik[2,4], S. Karan Venayagamoorthy[2], Timothy K. Gates[2], J.L. Marié[5]

[1] Univ. Grenoble Alpes, CNRS, Grenoble INP, LEGI, 38000 Grenoble, France.

[2] Department of Civil and Environmental Engineering, Colorado State University, Fort Collins, CO 80523-1372, USA.

[3] Physics and Engineering Department, Fort Lewis College, Durango, CO, 81301,USA

[4] College of Oceanic and Atmospheric Sciences, Oregon State University, Corvallis, OR 97331-5503, USA

[5] LMFA, UMR 5509, Univ. Lyon, CNRS, Ecole Centrale de Lyon, INSA Lyon, Université Claude Bernard Lyon 1, France.

Abstract

A developing narrow open-channel flow has been investigated using Acoustic Doppler Velocimetry (ADV) and Laser Doppler Anemometry (LDA). The objectives were to first characterize the flow environment with the LDA system alone, then quantify the intrusion effect of the ADV sensor immersion, and finally compare ADV-LDA measurements. The main features of the flow have been described. The turbulence levels measured in the outer flow are high and almost isotropic due to the specificities of the flow (3D, narrow, developing). This contributes to a flattening of the mean streamwise velocity profile in this region. The intrusion effect of the ADV sensor is found to be Froude number dependent ($Fr = U_0/\sqrt{gH}$ with U_0 the discharge velocity, H the flow depth, and g the gravity acceleration). Vertical flow below the sensor is amplified while the streamwise component of the flow is enhanced for "low" Fr numbers ($Fr \leq 0.6$) and reduced for "high" Fr numbers ($Fr \geq 1.1$). On the other hand, turbulent quantities are not affected by the sensor presence. Compared to the LDA, the ADV is shown to underestimate the mean flow and turbulent intensities, while not affecting Reynolds shear stress measurements. The underestimation of the turbulence intensities can be attributed to the lower sampling rate and larger sampling volume of the ADV, but the under-estimations of the mean velocities are more likely linked to a constant bias that the ADV seems to have or to some type of ADV-intrinsic noise. Some implications for practical application are discussed.

1 Introduction

Uncertainty and detection error are omnipresent facts for all field and laboratory measurements, including those concerning fluids. Attempts to observe undisturbed behavior of fluid flows have taken scientists and engineers beyond mechanical devices to electromagnetic, laser, and acoustic technologies. The Acoustic Doppler Velocimeter (ADV) has emerged over the past couple of decades as a popular device among laboratory and field scientists [Lohrmann et al., 1994]. The ADV functions using the acoustic Doppler principle. It emits acoustic signals of a known frequency, and detects the Doppler-shifted frequency reflected off particles that pass through the ADV sample volume, from which fluid velocity is determined [Tropea and Yarin, 2007, Aberle et al., 2017, Muste et al., 2017]. The ADV can provide a durable, user-friendly and affordable field alternative to other precision measurement devices like the laser Doppler anemometer (LDA), hot filament anemometer (HFA) or particle image velocimetry (PIV). ADV applications are wide ranging from oceanography [Lohrmann et al., 1995], aquatic ecology [Delavan et al., 2017] to river mechanics [Dey et al., 2017], irrigation canal flow accounting [Martin and Gates, 2014], estuarine dynamics [Chanson et al., 2008] and wake mechanics [Chen et al., 2017]. Mean velocity measurements and turbulent statistics measured by the ADV are shown to generally agree with those from the LDA, HFA and PIV despite some limitations and reduced performances near boundaries or behind obstacles [Finelli et al., 1999, Rusello et al., 2006, Dombroski and Crimaldi, 2007, Chara and Matousek, 2010, Poindexter et al., 2011, Khorsandi et al., 2012, Quaresma et al., 2017]. Its popularity has warranted detailed studies of error sources [Voulgaris and Trowbridge, 1998, McLelland and Nicholas, 2000]. Some of the intrinsic drawbacks of ADV measurements lay in spatial and temporal resolutions that are most of the time less accurate (larger sampling volume extent, lower sampling frequency) than when obtained with the above mentioned technologies. Inaccurate reporting of sample volume extent and location [Precht et al., 2006], and post-processing methodology [Romagnoli et al., 2012, Goring and Nikora, 2002] are also to be considered. The ADV is often considered as a non-invasive measurement device, due to the sample volume being some distance from the probe, unlike the HFA or mechanical flow meters. However, the assumption that the ADV probe has no effect on the flow passing through its sample volume has yet to be assessed. We address this issue for a developing narrow open-channel flow in a recirculating flume. Under different flow regimes we compared the measurements obtained for the streamwise and wall-normal (vertical) mean flow components as well as the turbulent quantities with an ADV and LDA [Buchhave et al., 1979, George and Lumley, 1973]. We do this with and without the ADV in the water so as to quantify the impact of the presence of the sensor in the flow together with the measuring differences between the devices. In what follows, the experimental setup and measuring devices are discussed first. This is followed by the characterization of the flow that is used. The influence of the presence of the ADV sensor is then investigated by comparing the LDA measurements with the ADV sensor in the flow and without. Finally, comparison of concurrent ADV and LDA measurements for the same flow conditions are presented.

2 Experimental setup and measuring devices

Experiments were conducted in an Armfield 5-m long, 0.3-m wide reclining from horizontal position, recirculating flume in the Environmental Fluid Mechanics Laboratory at Colorado State University, USA. The flume had a smooth metal boundary and glass siding as shown in Figure 1-left. The fluid was tap water at room temperature seeded with 20 μm Dantec

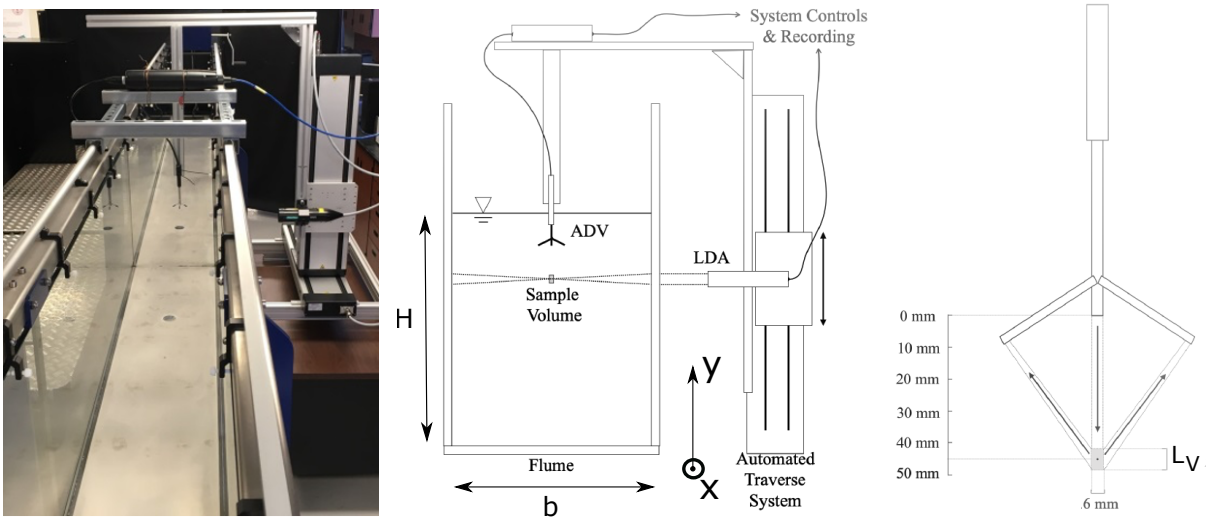

Figure 1: Left: Photograph of the experimental and measuring devices; middle: conceptual diagram of the experimental system; right: outline of the ADV measuring principle.

neutrally buoyant polyamid seeding particles. As will be outlined in the following, different flow regimes have been carried out for $Re = U_0 H/\nu \in [3.7 \times 10^4; 1.2 \times 10^5]$ and $Fr = U_0/\sqrt{gH} \in [0.2; 1.8]$ where H is the flow depth at the measuring location, ν is the kinematic viscosity of water, g is the gravitational acceleration, and $U_0 = Q/(Hb)$ is the discharge velocity with Q the flow rate and b the width of the flume. Velocity measurement was performed with both ADV and LDA measuring devices. The devices were positioned in the central cross section of the flume at about 4m from the entrance of the channel. The positioning and horizontality of the two measuring devices (LDA and ADV) was carefully and separately ensured both at installation and while running the experiments. Horizontality was checked using a spirit level. The relative alignment of the LDA with the flume was achieved by checking on the sides of the channel that the two laser beams of the horizontal plane were at the same distance from the bed. The LDA used was made of a Dantec 2D Fiberflow diode pumped solid state laser, emitting two 1.35 mm diameter beams at an output power of 100 mW each. Wavelengths of 491 nm for the vertical velocity component, and 515 nm for the horizontal one were used. A Dantec FiberFlow 60 mm probe was used with a focal length of 398.4 mm for both the beams, and a beam spacing of 38.302 mm and 38.306 mm for the vertical and horizontal components respectively. Signals were processed using a Dantec BSA F1600 processor and the instrument was operated with Dantec BSA Flow software. The lasers intersected to yield a measuring volume calculated by the BSA software for our optical set-up of 0.18 mm diameter and 3.87 mm length that leads to an equivalent diameter $L_{LDA} = 0.5\,mm$. The

corresponding viscous scaled LDA sampling volume typical length $L^+_{LDA} = L_{LDA}u_\tau/\nu$ (see Table 1) is of the order of values that are commonly found in past studies of wall or flume turbulence [Hutchins et al., 2009, Peruzzi et al., 2020]. LDA sample frequency was adapted for each velocity range to ensure both a good sample size and a high validation rate. Typical average sample frequencies for full profiles are summarized in Table 1. Very scarce (less than 1%) uncharacteristically high and low velocities were addressed by removing all data outside +/- 4 standard deviations of each sample's arithmetic mean. The ADV used in this study is a Nortek Vectrino I downward facing probe. Before using the ADV probe for measurements, the actual ADV sampling volume location was determined. [Finelli et al., 1999, Precht et al., 2006]. For our Nortek Vectrino I, this location was found to be 4.4 cm away from the ADV sensor (i.e., 6 mm higher than the nominal location indicated by the manufacturer). Sample rate, transmit length, and sample volume height were adjusted in each flow condition to settings that maintained a correlation coefficient (COR) larger than 70 and signal-to-noise ratio (SNR) larger than 15 dB [Dey et al., 2017]. The equivalent diameter L_{ADV} can be linked to a viscous scaled ADV sampling volume typical length $L^+_{ADV} = L_{ADV}u_\tau/\nu$ that happens unsurprisingly to have values larger than the ones reported for LDA (see Table 1). In the choice of the parameters we made sure that no ADV-measurement was contaminated by interference with the ADV's signals echoing off the bed [Dombroski and Crimaldi, 2007]. ADV settings at various flow conditions are summarized in Table 1. As previously reported for LDA and in the same way, uncharacteristically high or low velocity measurements were addressed by removing all data outside +/- 4 standard deviations of each sample's arithmetic mean. Both instruments were fixed to an Isel two dimensional automated traverse system (see Figure 1-left and middle) which was controlled using the Dantec BSA Flow software. The LDA focal point was positioned at the center of the ADV's nominal sample volume, which is typically 5 cm below the ADV probe, at the same stream-wise and span-wise position as the ADV probe. Since both instruments were rigidly attached to the traverse system, the two instruments moved in tandem during the experiments. Sample time was determined by monitoring time series of both instruments. A 4-min sample time was determined to be long enough for the sample variances to converge. Measurements were made on up to 18 points on the vertical axis to obtain so-called full profiles of both the streamwise and wall-normal (vertical) velocities. The purpose was to get a detailed view of the effect of the presence of the sensor in the flow as well as the difference in measurements between the ADV and the LDA as a function of H, Re, and Fr. Given the large time requirement for measuring the full profiles, we also performed less detailed measurements based on only three points vertically spaced so as to enhance the cartography of the results in the Re-Fr region as shown in Figure 2-left.

Given the ADV nominal sample volume being 5 cm below the ADV probe, a minimum H value of 7 cm has to be maintained in order to obtain measurements using the ADV. The Isel span imposed a maximum H of 18.25 cm. As such, these values of H delimit the $Re - Fr$ region that could be explored during this study.

3 LDA flow characterization

The first step of the study was to characterize the flow using the non-intrusive LDA (LDA_{wo}), without the ADV sensor immersed. As aforementioned, measurements were carried out in a section located about 4 m from the entrance and 1m from the exit. Referring to the work of

Table 1: Typical measuring device's characteristic features for full profiles. H: flow depth, b: flume width, U_0: discharge velocity, V_0: minimum of the vertical velocity measured. u_τ: bottom shear velocity, $Re_\tau = u_\tau H/\nu$: Reynolds number based on wall shear velocity, $Re = U_0 H/\nu$: Reynolds number based on average flow quantities, $Fr = U_0/\sqrt{gH}$: Froude number based on average flow quantities, S_0: flume tilt. f_{LDA}: typical average sample frequencies for LDA, f_{ADV}: sampling frequency set for ADV. L_y: ADV sampling volume height. $L^+_{ADV} = L_{ADV} u_\tau/\nu$: viscous scaled ADV sampling volume typical length, $L^+_{LDA} = L_{LDA} u_\tau/\nu$ viscous scaled LDA sampling volume typical length. Green symbols come for experiments with a tilted flume.

Exp #	1	2	3	4	5	6
$H(cm)$	15	15	15	15	15	10
b/H	2	2	2	2	2	3
$U_0(m/s)$	0.25	0.4	0.5	0.67	0.78	1.17
$V_0(cm/s)$	-0.8	-1	-1.3	-2.8	-4.9	-7.4
$u_\tau(cm/s)$	1.3	2	2.5	3.3	4	6
$Re_\tau(\times 10^3)$	2	3	3.8	5	6	6
$Re(\times 10^4)$	3.7	6	7.5	10	11.7	11.7
Fr	0.2	0.3	0.4	0.5	0.6	1.2
tilt (S_0) (°)	0;1/200[a]	0	0	0	0	1/200
$f_{LDA}(Hz)$	40	120	200	200	400	500
$f_{ADV}(Hz)$	40	50	100	75	100	100
$L_y(mm)$	4	7.6	2.5	4.3	2.5	2.5;4[b]
L^+_{ADV}	70	160	100	180	150	230;310
L^+_{LDA}	7	10	10	20	20	30
Symbols	x: no tilt, x:tilt	▽	○	◁	□	▷

[a] Experiment 1 has been run twice with 2 different flume inclinations. Only mean velocities and shear stress has been kept for presentation for the tilted one since the LDA results for these low recirculating rates exhibit higher level of noise on the fluctuating quantities likely in relation with a lower amount of seeding particles.

[b] Experiment 6 has been run twice with 2 different sampling volume lengths for ADV.

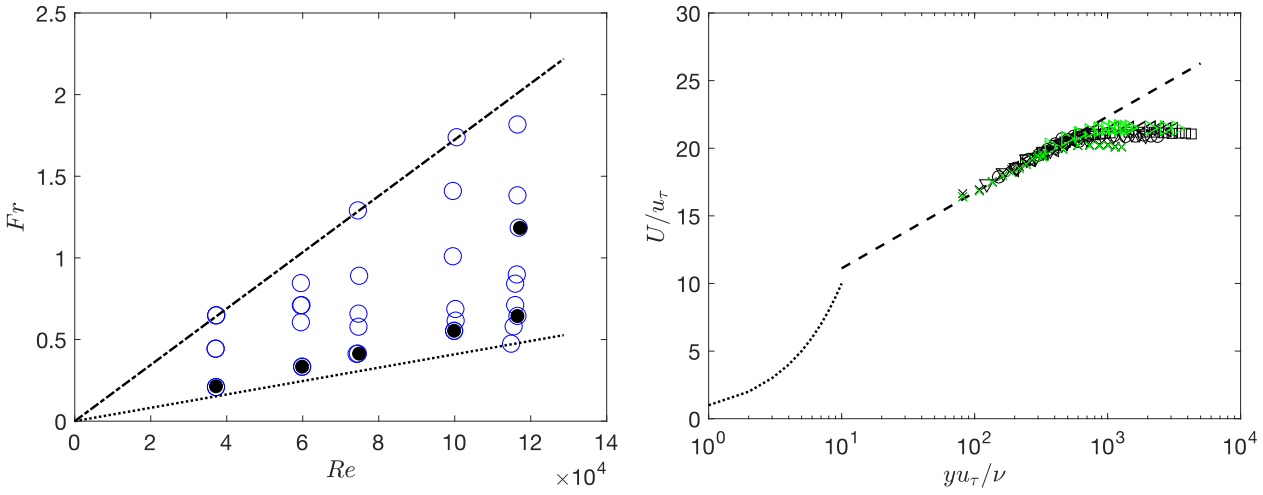

Figure 2: Left: $Re - Fr$ region explored. Black dots: "full" profiles, blue circles: 3 points profiles. Dotted line: region limit due to $H_{max} = 18.25\,cm$, dashed-dotted line: region limit due to $H_{min} = 7\,cm$. Right: dimensionless streamwise velocity profile. See Table 1 for symbols. Dotted line: viscous layer law, dashed line: log-law for channel flows.

Kirkgöz and Ardiçlioğlu [1997], this distance is small compared to the length L required for the open channel flow to be fully developed. Indeed, using the correlation proposed by these authors to estimate the developing length L, as function of Re and Fr with the data reported in Table 1, we find that L ranges between 6.6 m for Exp 6 and up to 8.6 m for Exp 1. This suggests that our measurements are obtained in the developing zone, where the boundary layer developing on the bed has not yet reached the free surface (see figure 1 and 4 in Kirkgöz and Ardiçlioğlu [1997]). This is all the more true given that the boundary layer on the bed is not triggered at the entrance. On the other hand, the flows investigated are also non-uniform. The depth decreases slightly with x ($\approx$ 0.01m over 5m at maximum for high Re) implying that the flow is accelerating. The level of non-uniformity can be evaluated by the pressure gradient parameter β [Clauser, 1956, Mellor and Gibson, 1966] defined in open channel flows [Kironoto and Graf, 1998, Peruzzi et al., 2020] as

$$\beta = \frac{gH(x)}{u_\tau^2(x)}\left(\frac{dH}{dx} - S_0\right) \tag{1}$$

$u_\tau(x)$ being the shear velocity estimated from bulk-momentum balance. In our case the order of magnitude of β is estimated to lie in between -2 and -3. Its evolution along x has not been measured and so it was not possible to conclude whether the flow is in equilibrium (β constant). The so-called full profiles results obtained for each of the six Re numbers investigated are plotted under the standard non-dimensional inner-layer form in Figure 2-right. It can be seen that the lower points of the measured profiles lie in the log-law region. In this figure, u_τ denotes the shear velocity and U is the streamwise velocity component at a vertical height y above the flume bed. Given the difficulty in measuring the wall shear stress directly, we derived the shear velocity u_τ by means of the Clauser method [Clauser, 1956, Wei et al., 2005]. The method is based on the assumption that an overlap region exists close to the wall, where the

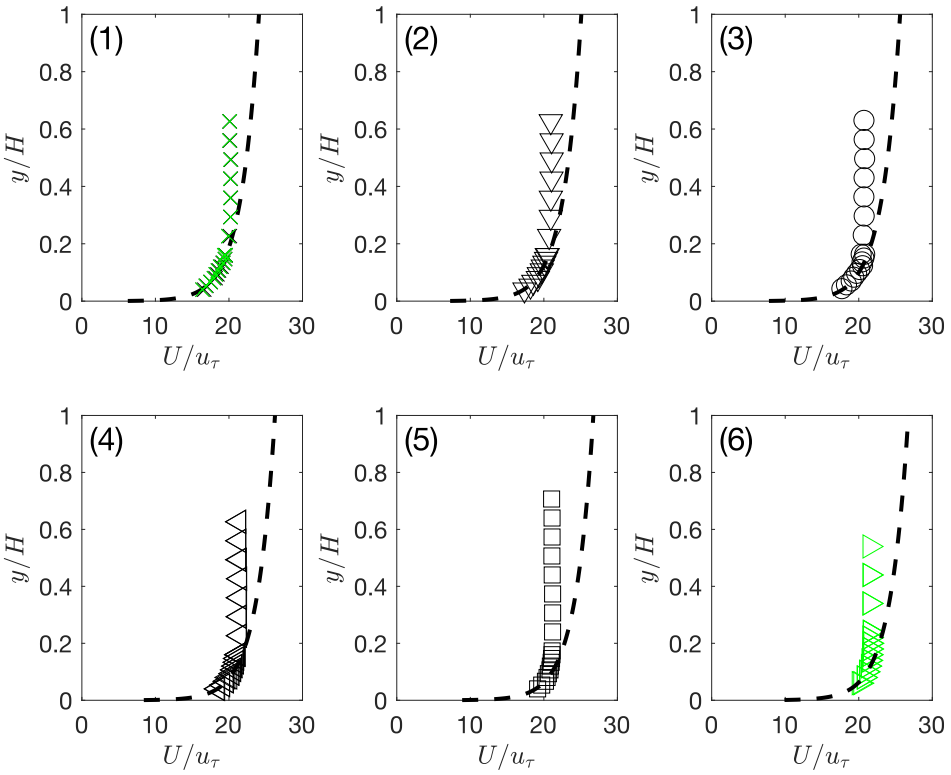

Figure 3: Dimensionless mean streamwise velocity profiles. See Table 1 for symbols and experiment number (between brackets). Dashed line: log-law for channel flows.

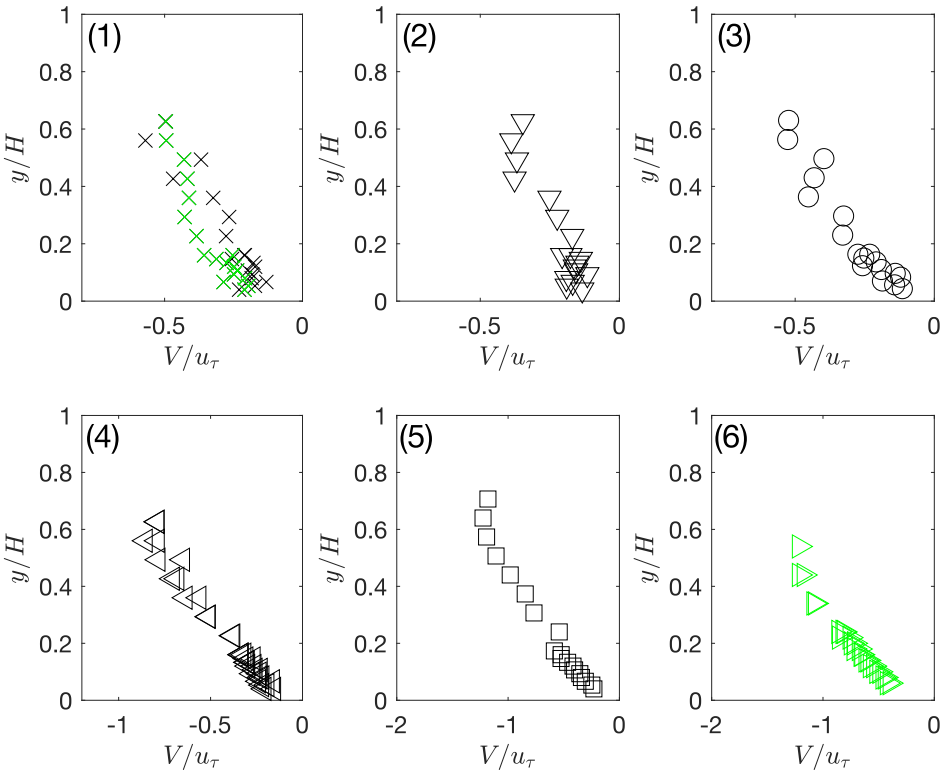

Figure 4: Dimensionless mean vertical velocity profiles. See Table 1 for symbols and experiment number (between brackets).

streamwise mean velocity follows a logarithmic behaviour such as:

$$\frac{U}{u_\tau} = \frac{1}{\kappa} ln\left(\frac{yu_\tau}{\nu}\right) + C. \tag{2}$$

where $\kappa = 0.41$ is the von Kármán constant and $C = 5.5$ is the additive constant for flume flows [Gad el Hak and Bandyopadhyay, 1994, Kirkgöz and Ardiçlioğlu, 1997, Peruzzi et al., 2020]. This assumption turned to be rather well validated in uniform and non-uniform open-channel flow, even when aspect ratio is low like in the present study [Kirkgöz and Ardiçlioğlu, 1997, Kironoto and Graf, 1998]. Practically u_τ was estimated from the best least-square fit of our data to equation (2). This fit was performed on 11 points for $y+ = \frac{yu_\tau}{\nu}$ between approximately 100 and 400 for the lowest Re and 4 points between approximately 400 and 700 for the highest Re. The uncertainty in the wall shear velocity thus depends on Re. It can be estimated to be 0.5% at low Re and 0.8% at high Re. The values of u_τ obtained are reported in Table 1. As can be seen, most of the upper points of the profiles are located outside the log region and no wake effect can be detected [Coles, 1956]. The velocity profiles there become flat with a maximum velocity that is more or less accentuated depending on the Re number. Referring to Kirkgöz and Ardiçlioğlu [1997], the fact that the profiles are measured in the developing zone could explain the absence of the wake, but the results presented hereafter indicate that this is probably not the only reason. Each of these velocity profiles is plotted in Figure 3 as a function of the outer dimensionless distance y/H. Under that form, we see that the deviation of the profiles from the log law caused by the flattening takes place at y/H between 0.1 and 0.2, dependant on Re. The corresponding dimensionless mean vertical profiles, where V is the vertical velocity component at y, are reported in Figure 4 . We note that this vertical component is non-negligible and increases in absolute value with Re number. This significant vertical velocity arises due to various physical origins that combine together. One of these, is the small aspect ratio b/h of our open channel flow, between 2 and 3. It was observed that for b/h less than 5 [Nezu and Nakagawa, 1993, Shinneeb et al., 2021], narrow open-channel flows are three dimensional in the fully developed region. Strong re-circulation zones then form near the surface and the bottom that can induce vertical velocities in the channel mid plane. This holds for developed regions but we may expect that it also occurs in our measuring section. Another effect that could also amplify vertical velocities is the high level of turbulence in the free stream. This can be seen in Figure 5 and 6 which show the non-dimensional velocity fluctuations and Reynolds stress. u' denotes the streamwise velocity fluctuation from U, and v' the vertical velocity fluctuation from V. As expected, $u'/u_\tau \approx 2v'/u_\tau \approx 1$ within the logarithmic region, the flow being strongly influenced by the presence of the flume bed.

As the profile enters the outer layer ($y^+ = yu_\tau/\nu > 10^3$), horizontal and vertical fluctuations tend towards the same level ($u'/u_\tau \approx v'/u_\tau \approx 1$), indicating that turbulence returns to isotropy. This differs from other studies in flume flows which usually report turbulent anisotropic conditions $u'/u_\tau \approx 1, v'/u_\tau \approx 0.5$ in the outer layer [Roussinova et al., 2008, Peruzzi et al., 2020]. This difference can be attributed to the high intensity residual turbulence existing in the free-stream. This turbulence is the result of the 3D energetic flow structures generated upstream of the test section in the hydraulic circuit by the pump and the bend at the entrance. This residual turbulence, by increasing the momentum transfer, contributes to flattening the mean streamwise velocity profiles in the outer layer, similar to what happens in a turbulent boundary layer subjected to a free-stream grid generated turbulence [Hancock and

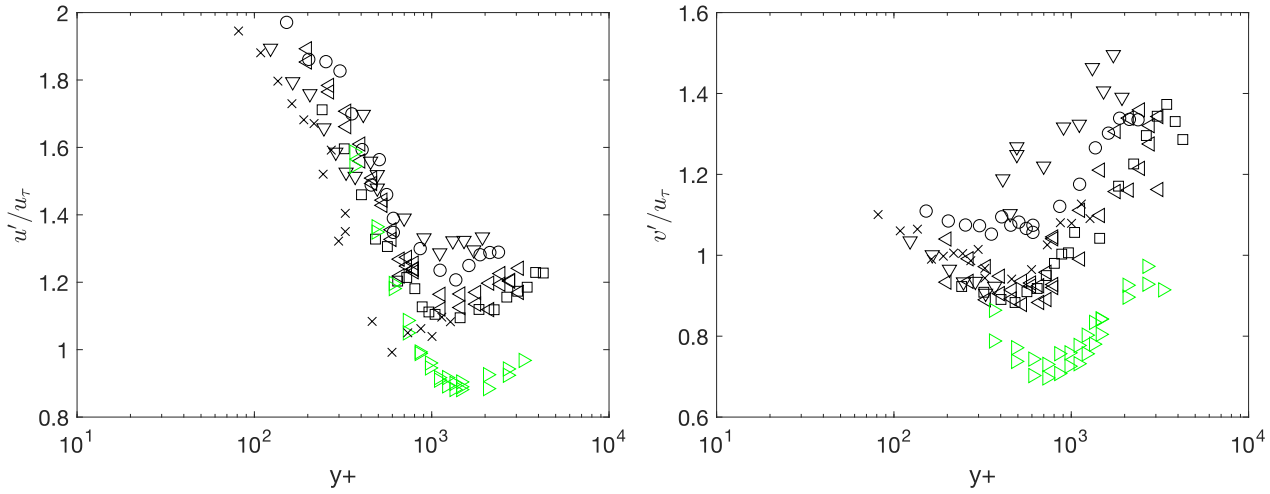

Figure 5: Left: dimensionless streamwise velocity fluctuations u'/u_τ versus $y^+ = yu_\tau/\nu$. Right: dimensionless vertical velocity fluctuations v'/u_τ versus $y^+ = yu_\tau/\nu$. See Table 1 for symbols.

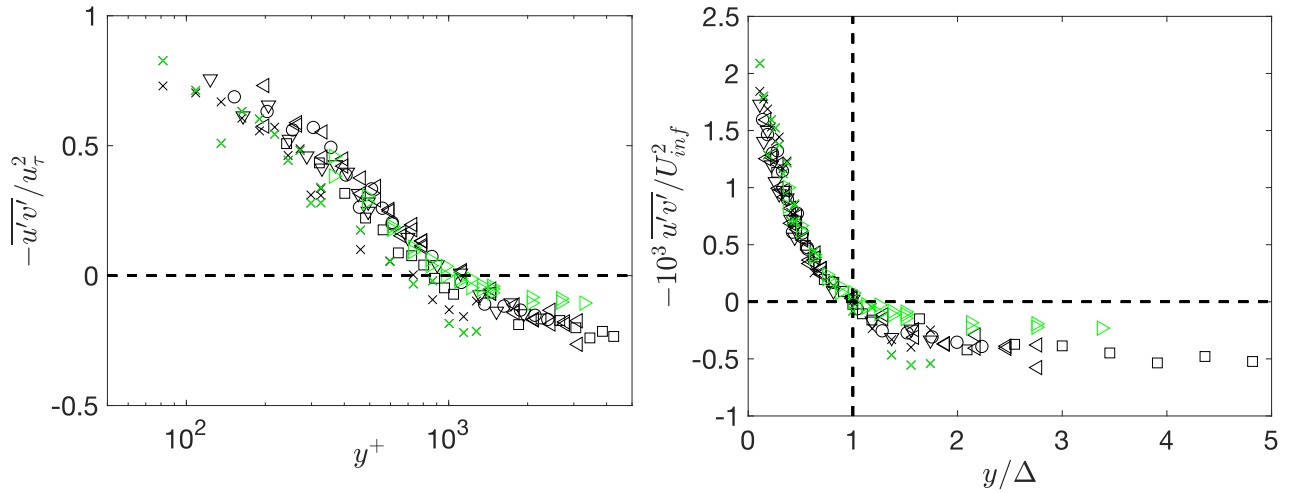

Figure 6: Left: dimensionless Reynolds shear stress versus vertical position using inner scaling. Right: non-dimensional Reynolds shear stress as a function of the outer scale y/Δ. Δ is the height where the Reynolds stress changes its sign and $U_{inf} = U(\Delta)$. See Table 1 for symbols.

Bradshaw, 1983, 1989, Sharp et al., 2009, Dogan et al., 2016, Jooss et al., 2021]. The parameters quantifying the effect of the free steam turbulence in these studies are the turbulence intensity (the effect increases with this intensity) and the ratio of its integral length scale over the boundary layer thickness (large scale turbulence has more effect). In our case the turbulence intensity in the free stream is almost constant and relatively high: between 6.3% and 6.5% across all tested values of Re, which may influence the development of the flow [Jooss et al., 2021] and modify significantly the Coles wake parameter Π [Dogan et al., 2016]. The absence of the wake is not the only questioning point in our flow. We see in Figure 5 that the Reynolds stress ($-\overline{u'v'}$) which is positive in the log-layer, becomes systematically negative in the outer layer. The same behaviour has been reported by Sarkar [2016] near the centre of a narrow open channel with an aspect ratio $b/H = 2$ comparable to the experimental setup of this study, meaning that it can be linked to flow re-circulations. But it can be also be connected with the free stream turbulence. The height Δ where the sign change in the Reynolds shear stress takes place can be viewed as the effective thickness of the boundary layer in the measuring section. Its use to scale the outer region of the flow is shown in Figure 6 and 7. We see in Figure 6-right that this scaling provides a remarkable collapse of all the Reynolds stress data. Also, we note the same good collapse in Figure 7-left for the streamwise deficit velocity profiles, with a minimum visible around $y = \Delta$ with $U_{inf} = U(\Delta)$. The additive constant in the log law $-2\Pi/K$ is about -1.5, that corresponds to a Coles wake parameter Π of the order of -0.3, a value which is consistent with the data of Dogan et al. [2016] ($\Pi = -0.26$, cases A and B table 2) for similar turbulence intensities. However, this negative wake parameter may also result from the non-uniformity of the flow. According to Kironoto and Graf [1998] a pressure parameter β of -2,-3 can yield a Π value of -0.16, -0.24 (0.08*β) for 3D flows with small aspect ratios. The typical height Δ is about the distance where the turbulence fluctuations become isotropic. It corresponds to the depth where the effects of the free stream turbulence extend into the boundary layer developing on the channel bed. In some respect, this scaling resembles that of Roussinova et al. [2008] based on a constant turbulence intensity close to the free surface for the outer layer. As we do not have sufficient data with a tilted flume no definitive tilt related statement should be made out of the observed behaviors. Nevertheless, figures 5, 6 and 7 appear to indicate that a tilt of the flume may have more influence on turbulence intensities than on mean flow or Reynolds shear stress. As the effect has not been observed for developed 2D-channel flows [Cameron et al., 2017] it is likely to be linked to the developing characteristics of our flow.

In summary, LDA measurements show that the flows investigated have a very specific structure (absence of the wake, significant vertical velocity, high free stream turbulence intensity, sign change of the Reynolds stresses), not representative of those characterizing fully developed open-channel flow generally studied in the literature. In that context, comparison between LDA and ADV is interesting since it highlights how the two metrologies behaves in such unfavorable specific situations. Also it means that the conclusions found from this comparison might not be considered as general and may not hold for all open channel flows situations.

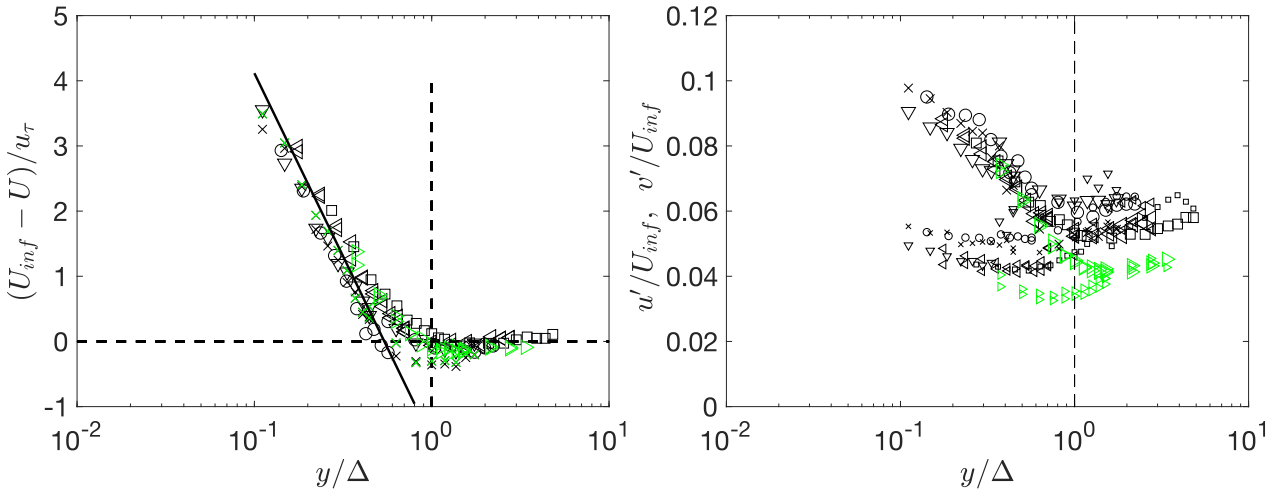

Figure 7: Left: deficit streamwise velocity profile in the defined outer scale scaling. Black plain line: $(1/\kappa) \times log(y/\Delta) - 1.5$. Right: dimensionless turbulent intensity profiles (u'/U_{inf}, v'/U_{inf}) as a function on y/Δ. Large symbols are for streamwise components and small ones for vertical components. See Table 1 for symbols.

4 ADV intrusion effect

The ADV sensor intrusion effect is studied for each of the six Re values previously investigated. Here we address the question, "How is the flow environment altered by the insertion of the ADV into the flow?" This is done by comparing LDA measurements at the same positions with and without the sensor immersed in the flow. LDA measurements with the ADV sensor are denoted by LDA_w, those without the sensor by LDA_{wo}. In what follows, subscript w is used for parameters measured in the first situation and subscript wo for those measured in the second one. The corresponding mean streamwise and vertical velocity profiles are compared in Figures 8 and 9, respectively. The plots labeled (1)-(4) in Figure 8 show that the streamwise velocity measured for the LDA_w case, U_w, is greater than the velocity U_{wo} measured for the LDA_{wo} case, whatever the position in the profile, indicating that the flow is accelerated by the presence of the ADV sensor. These four plots correspond to flows with a "low" Froude number ($Fr < 0.6$). Plots (5) and (6) correspond to higher Fr values ($Fr \in [0.6; 1.2]$) and show the opposite trend to the cases with low Fr ($U_w < U_{wo}$ regardless of the position), meaning that the flow decelerates in the presence of the ADV sensor. In the vertical direction (Figure 9), the mean velocity V_w is always greater than V_{wo} whatever the Froude number Fr, the difference between V_w and V_{wo} increasing with decreasing distance from the bed. From plot (1) in Figures 8 and 9, the flume tilt does not appear to have an impact on the overall behavior.

To confirm the above seen trends, extra experiments were performed with three points only instead of full profiles. The normalized velocity difference as a function of Fr can be seen in Figure 10-left (streamwise direction) and Figure 10-right (vertical direction). The extra measurements confirm that for $Fr < 0.6$ the sensor intrusion in the flow makes the mean flow accelerate in the streamwise flow direction with about a 3% increase. The region $0.6 < Fr < 1.1$ appears to be more flow-dependent with mostly mean streamwise flow

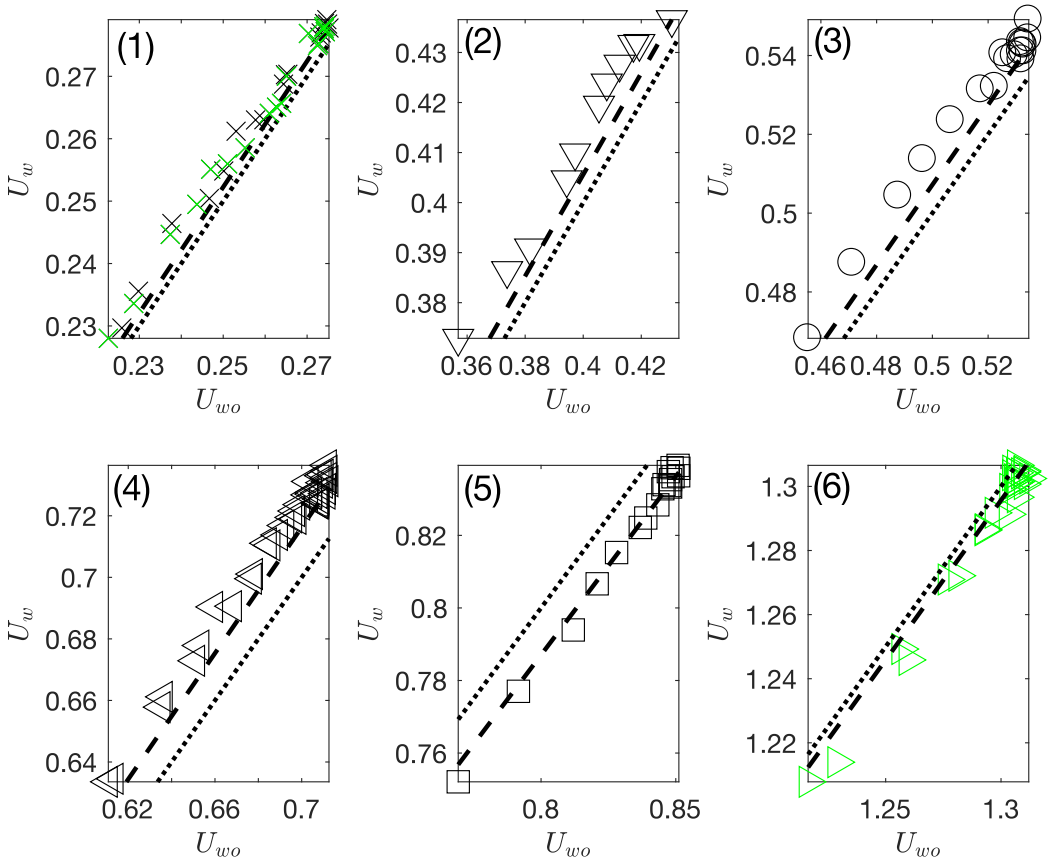

Figure 8: Mean streamwise velocity measured with the ADV sensor immersed as a function of the velocity without the sensor immersed at the same position in the profile. See table 1 for symbols and experiment number (between brackets). Dotted line: 1:1 slope, dashed line: slope U_{wM}/U_{woM} where U_{wM} and U_{woM} are the respective maximum streamwise fluid velocities with and without the ADV sensor.

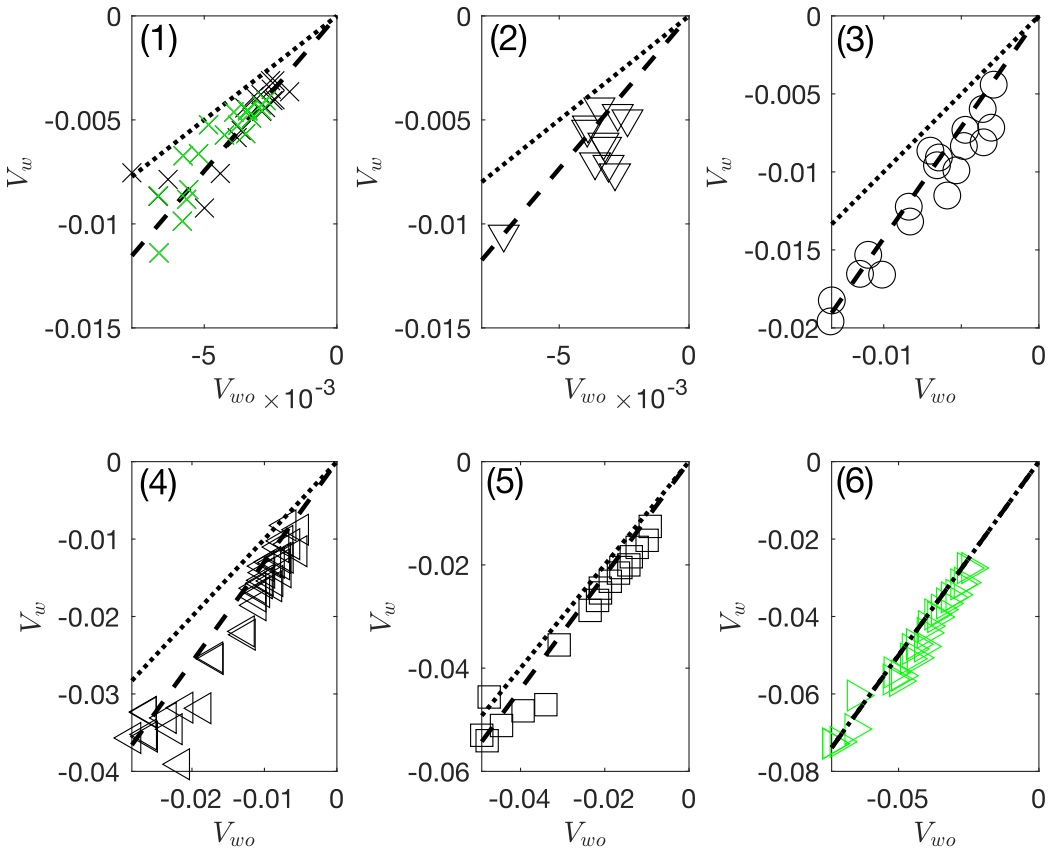

Figure 9: Mean vertical velocity measured with the ADV sensor immersed as a function of the velocity without the sensor immersed at the same position in the profile. See Table 1 for symbols and experiment number (between brackets). Dashed line: slope V_{wM}/V_{woM} where V_{wM} and V_{woM} are the respective minimum (negative) vertical fluid velocities, dotted line: 1:1 slope.

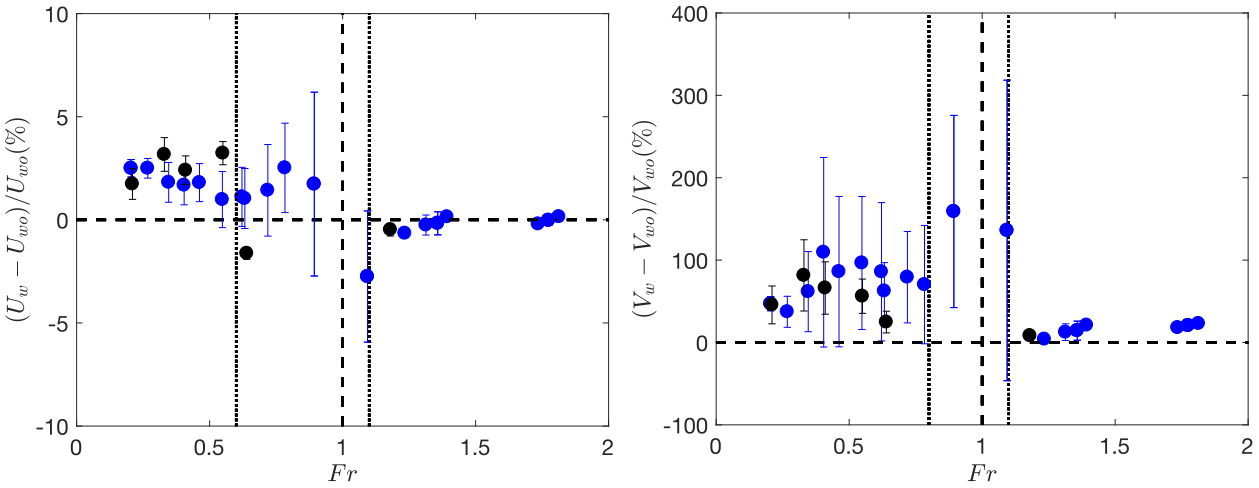

Figure 10: Dimensionless mean velocity difference versus Fr. Blue: three point measurements, black: full profile measurements. Left: streamwise velocity, right: vertical velocity.

accelerations but also with a couple of decelerations and increased standard deviations. For $Fr > 1.1$ the flow is bound to a reproducible tiny streamwise deceleration (less than 1%). As seen in Figure 10-right, the vertical component of the flow velocity V is affected more by the presence of the ADV sensor. Indeed, for "low" Fr numbers ($Fr < 0.6$), V increases like U, but in higher proportions that can reach 100% of the undisturbed vertical velocity. For "high" Fr numbers ($Fr > 1.1$), while U slightly decreases when the sensor is immersed, V still increases; however, this increase never exceeds 20%. One reason for this lower increase could be that the perturbation generated by the sensor is carried downstream more easily as inertia effects become dominant. The intermediate region ($0.6 < Fr < 1.1$) is the region where the sensor's presence most alters V, up to 150% for the points measured and even higher as Fr gets closer to 1.

These differences in behavior can be linked to the disturbances generated at the free surface by the ADV sensor, as seen in Figure 11.

- For low Froude numbers ($Fr < 0.6$: the image on top), the presence of the sensor is very weakly perturbing the free surface with only a thin wake behind the rod that holds the sensor. No noticeable flow depth modification is to be reported. In this case the sensor and the rod contribute to block the flow section, which induces a streamwise acceleration around the sensor components as a result of mass conservation principles. This conservation of steady flow rate can be written as

$$Q = U_0 Hb = U_s(Hb - S_s), \tag{3}$$

with U_s the discharge velocity at the sensor location and S_s the projected surface area of the sensor and of the holding rod perpendicular to the flow direction. This simplifies to

$$\frac{U_s}{U_0} = \frac{1}{1 - \frac{S_s}{Hb}}. \tag{4}$$

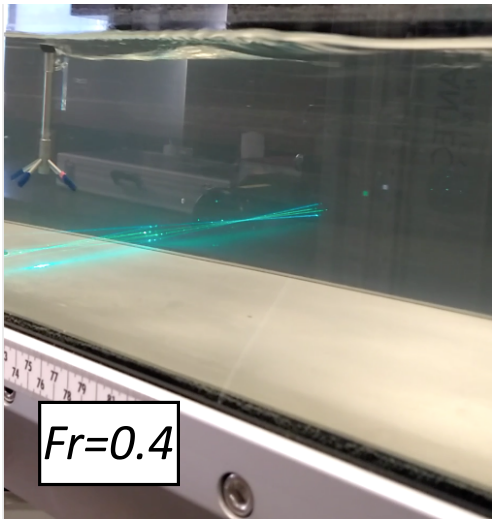

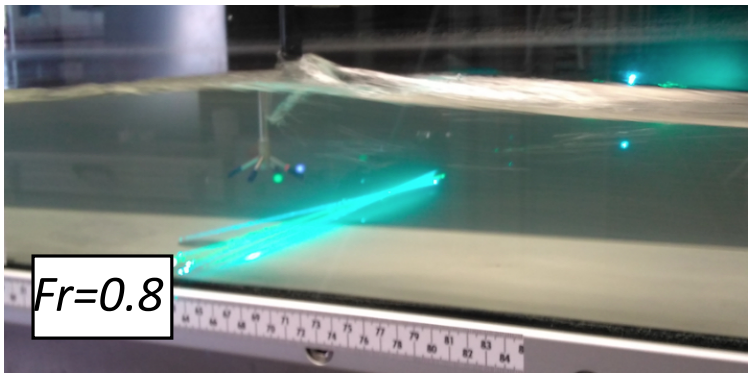

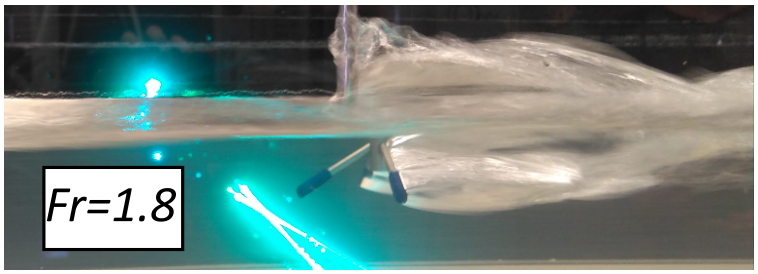

Figure 11: Typical flow modifications by the presence of the ADV sensor depending on the value within the Fr-range explored by either full profiles or three-point measurements. $Fr \leq 1.1$ single-phase regime, $Fr > 1.1$ two-phase regime.

Since the sensor is always fully immersed in the flow, its projected surface does not change whatever the position in the profile and is easily calculated given the manufacturer property sheets. On the other hand, the holding rod part of the projected surface area varies with the measuring position. This depth is more or less important depending on if the measurement is performed closer to the flume bed or to the free surface. Knowing the measuring depth, it is easy to compute the projected surface area of the rod. This surface area varies linearly with the measuring location y from the bed. The influence of this blocking effect on U_s/U_0 (equation 4)) can be seen in Figure 12 for the streamwise velocity profiles U_w and U_{w0}. Velocities have been non-dimensionalized by the maximum streamwise velocities U_{woM} and U_{wM}, measured in each of the two situations, so as to remove of Fr effects on the vertical axis. It is interesting to note that the behavior expected from equation (4) for U_s can therefore also be observed on the velocity profiles. As expected, the overall is in favor of an intrusion effect that is more important for narrow flumes than for large ones.

- In the intermediate range ($Fr \in [0.6; 1.1]$: the image in the middle) the presence of the sensor perturbs the free surface. An overall bump in the free surface at the sensor's location together with, in some cases, a hole before or after the sensor was noticeable. The flow depth can be up to 10% higher than the undisturbed depth over the whole width of the flume. Its impact on the LDA measurements is strongly dependent on Fr and thus would require more detailed measurements to enable a better understanding. As above mentioned, this is typically the range where the sensor's presence by inducing this bump in the free surface most alters V (Figure 10-right).
- Larger Froude numbers ($Fr > 1.1$: the image on the bottom) see the free surface recovering a flat shape upstream of the sensor rod. On the other hand, a strong wake develops downstream of the sensor attached to the whole sensor/rod device. The depression induced by this wake is sucking air at the free surface, thus forming large bubbles that remain trapped in the low pressure regions of the wake (behind the rod, behind each one of the sensor receivers). The size of these bubbles is representative of the size of the region that is directly affected by the presence of the sensor. The lengths of the bubbles have been measured by direct observation when present (for high Fr experiments). Their order of magnitude has been chosen as a characteristic scale (L_{wake}) for describing the impact of the sensor on the flow in this situation. The main effect of the wake and the bubble trapped within it is to decelerate the flow (see plots (5) and (6) in Figure 8). From Figure 13, we see that the observed slow-down of the flow is almost constant when the measured position from the flume bed is of the order or greater than L_{wake}, while it slightly increases as this position is smaller. The result is that the scaling with L_{wake} and U_{woM}/U_{wM} provides a good collapse of our data for the two decelerations linked with the values of Fr investigated.

To better quantify the Fr evolution of the profiles U_w versus U_{wo} in Figure 8, we show on the left in Figure 14 a plot of the ratio of the maximum streamwise velocities U_{wM}/U_{woM} used to scale these profiles in Figures 12 and 13, as a function of the Fr number. It can be seen that for $Fr < 0.6$, this ratio is greater than 1 and increases almost linearly with Fr (the flow is accelerated by the presence of the ADV sensor), while for $Fr > 0.6$ the trend is inverted and the flow is slowed-down by the sensor (ratio < 1). It is noted that the value of

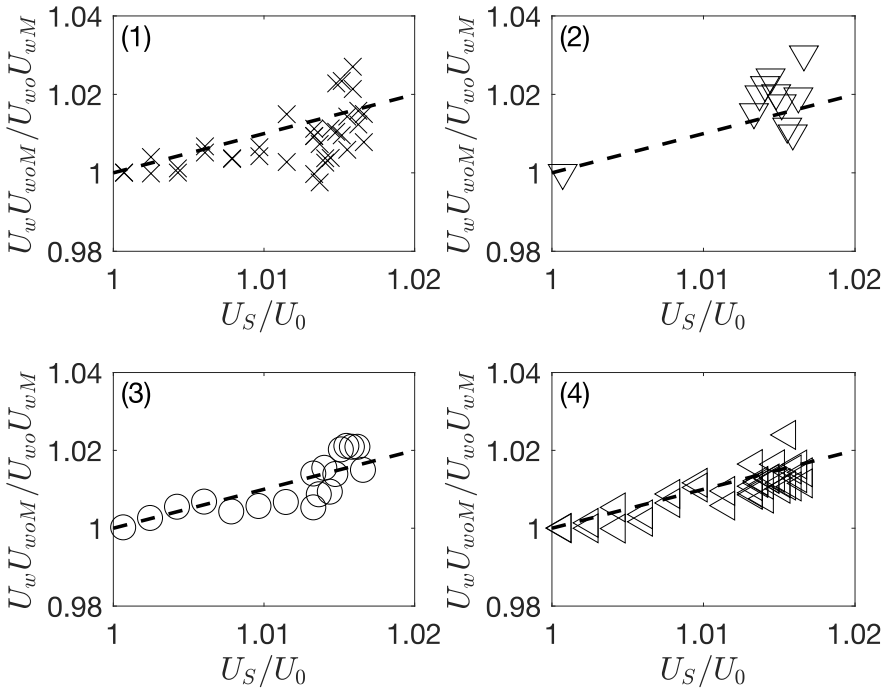

Figure 12: Dimensionless streamwise velocity ratio between measurements with the sensor immersed and not immersed as a function of U_s/U_0. See Table 1 for symbols and experiment number (between brackets).

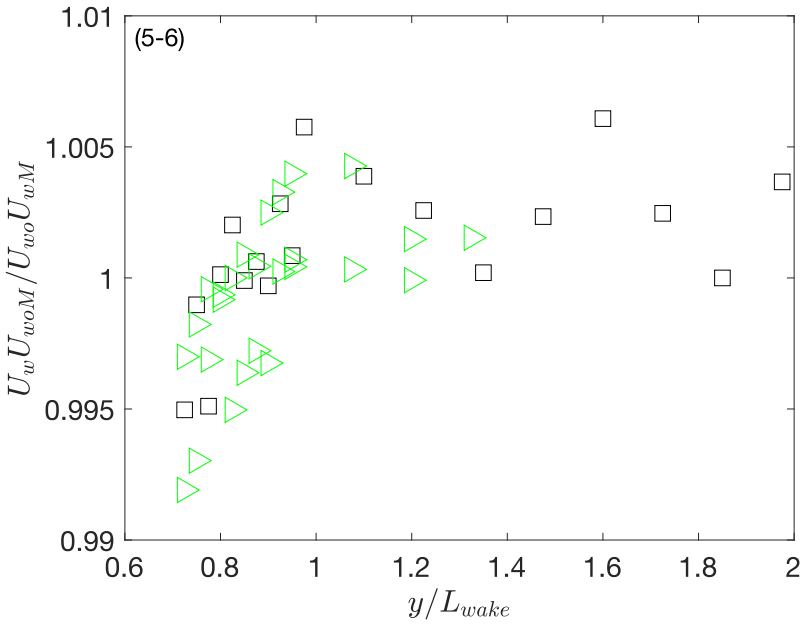

Figure 13: Dimensionless streamwise velocity ratio between measurements with the sensor immersed and not immersed as a function of the vertical position compared with the wake sucked in bubble size. See Table 1 for symbols and experiment number (between brackets).

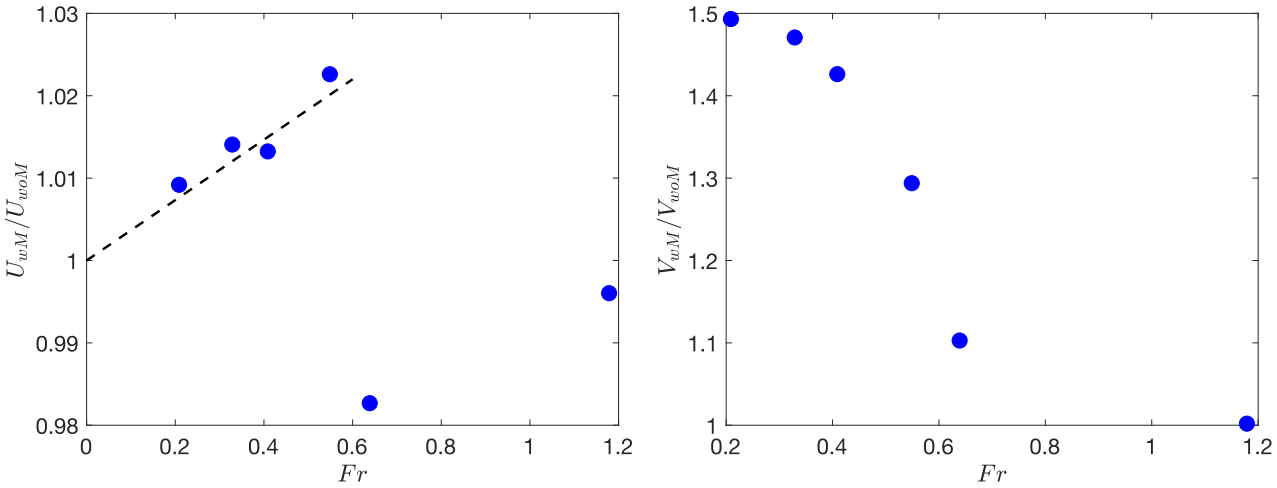

Figure 14: Left: maximum streamwise velocity ratio versus Fr. Line: $1 + 0.022 \times (Fr/0.6)$. Right: maximum vertical velocity ratio versus Fr.

U_{wM}/U_{woM} found for each of the Fr numbers is illustrated by the slope of the dashed lines in Figure 8 onto which the profile data collapse well. This suggests that the intrusion effect on the streamwise component of the flow seems to be rather independent of the position in the profile (inner or outer region). As for U, the Fr influence on V has been quantified by plotting the ratio between the maximum vertical velocities V_{wM} and V_{woM} of the V profiles measured for each Fr, with and without the ADV sensor (see Figure 14-right). For $Fr < 0.6$ a smooth decrease is evident as Fr increases, with inertia effects becoming more important. As for U, the value of V_{wM}/V_{woM} that corresponds to each Fr value, is the slope of the dashed lines in Figure 9 on which the data are collapsing fairly well.

However, as shown in Figure 15, the turbulent stresses are not affected by the presence of

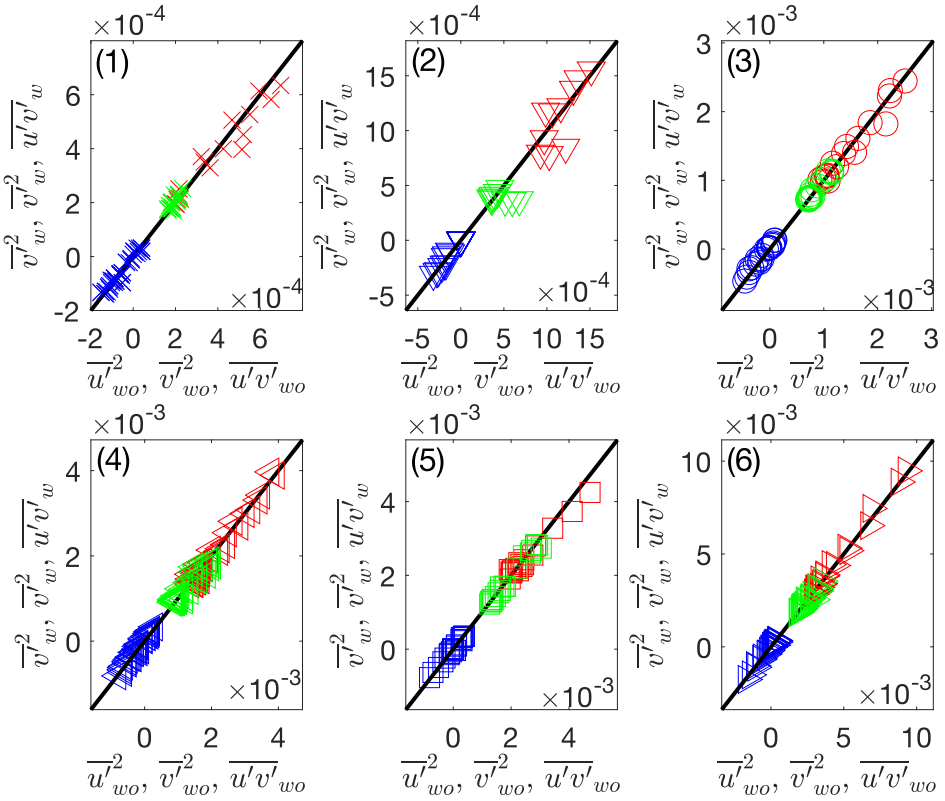

Figure 15: $\overline{u'^2}$ (red), $\overline{v'^2}$ (green) and $\overline{u'v'}$ (blue) measured with the sensor immersed as a function of $\overline{u'^2}$, $\overline{v'^2}$ and $\overline{u'v'}$ without the sensor immersed at the same position in the profile. See Table 1 for symbols and experiment number (between brackets). Plain line: 1:1 slope.

the sensor. All measurements collapse onto the 1 to 1 slope line shown in Figure 15. This result is significant as it highlights that the intrusion effects of the ADV on turbulent quantities appears to be negligible. This is confirmed by the comparison of the turbulent kinetic energy spectra for both measurements (see Figure 16). Spectra obtained for the measurements without the sensor immersed and spectra with the sensor lay on top of each other both for the streamwise and the vertical velocity components. A turbulent slope of $-5/3$ is observed in the power

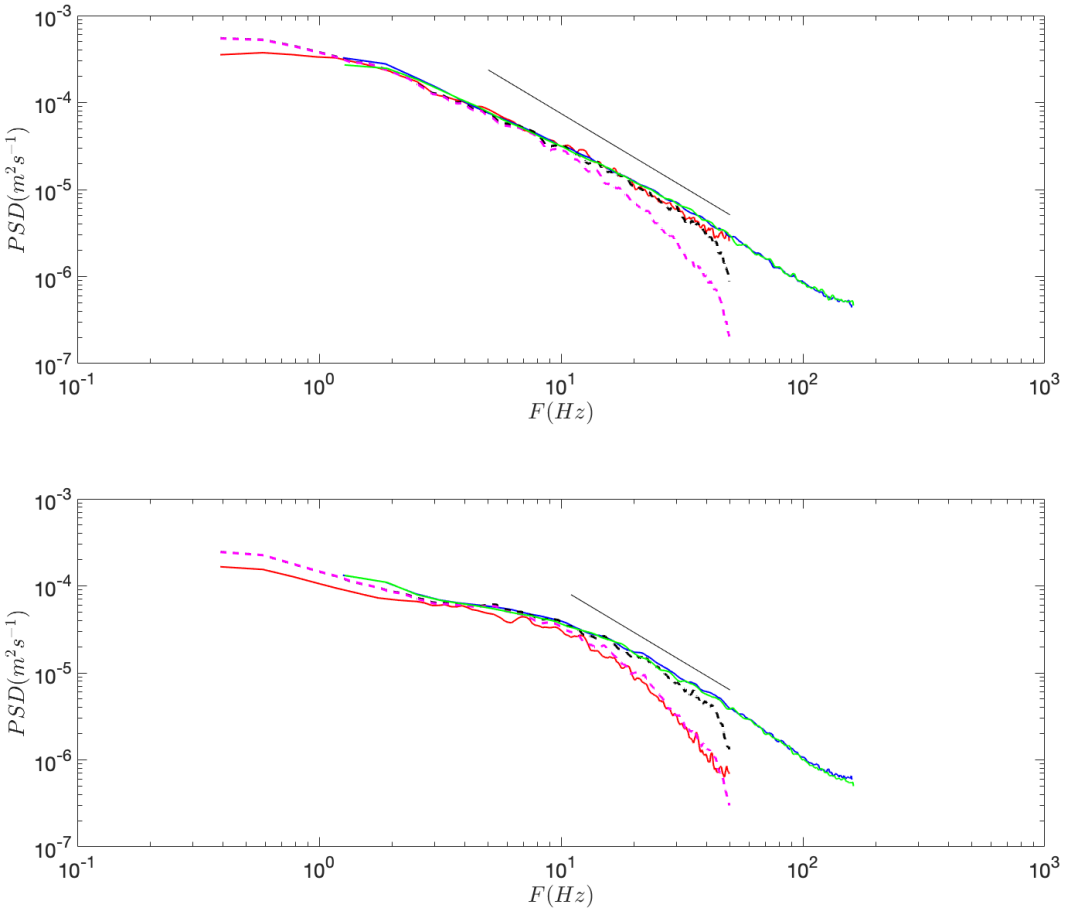

Figure 16: Temporal turbulent kinetic energy spectra as a function of frequency. Spectra from Exp5 and $y/\Delta = 1.1$. Top: streamwise component, bottom: vertical component. Green plain line: LDA measurement without the ADV sensor in the flow. Blue plain line: LDA measurement with the ADV sensor in the flow. Red plain line: ADV measurement. Black: LDA measurements degraded through the three steps procedure with $N = 2$ (see section 5), Magenta: LDA measurements degraded through the same procedure with $N = 5$. Black solid line: slope -5/3.

spectra density functions (PSD) as a function of frequency (F).

5 ADV versus LDA measurements

After characterizing the flow environment (Section 3) and estimating the intrusion impacts of the ADV sensor (Section 4), we now directly compare the measurements obtained by the two techniques for the same flow situations. The questions addressed here are, "what are the net differences between the turbulent open-channel flow characteristics measured by the ADV and those measured by the more precise and non-intrusive LDA in the same fluid environment?" and "what are the reasons for these differences?" In the first two parts involving results (flow characterization and influence of the intrusion of the sensor in the fluid), Re and Fr have appeared as key non dimensional numbers governing the observed behaviors. Therefore, we presented the results in a detailed Re and Fr way. However, we find that the differences in instrument measurements (ADV vs LDA) is not significantly influenced by Re nor Fr numbers. As a consequence, we chose to present some of the flow profiles that were quantitatively the most representative of the differences observed between the ADV and the LDA. As reported in Section 2 and Table 1, the ADV settings were chosen according to the flow velocities range within the flume together with high COR and SNR. As shown in Figure 17 and Table 2, the

Table 2: Average relative deviations (indicated by the symbol Δ) between the ADV and LDA_w measurements. From left to right: streamwise and vertical mean velocities, streamwise and vertical fluctuating intensities, and Reynolds shear stress correlation coefficient.

$\Delta U/U$	$\Delta V/V$	$\Delta\overline{u'}^2/\overline{u'}^2$	$\Delta\overline{v'}^2/\overline{v'}^2$	$\Delta\overline{u'v'}/\overline{u'v'}$
-3%	-30%	-15%	-60%	10%

ADV is systematically underestimating the mean streamwise and vertical velocities measured by the LDA, confirming previous findings by Chara and Matousek [2010] and Dombroski and Crimaldi [2007] who for the mean streamwise component find deviations of the order of -7% and -5%, respectively, which are comparable to our measured results. Dombroski and Crimaldi [2007] attribute the mean velocity biases far from the flume bed to the ADV averaging spatial gradients and to some "combination of factors related to the sample volume size". The fluctuating streamwise and vertical intensities are also weaker when measured using the ADV compared to the LDA, in accordance with Dombroski and Crimaldi [2007]. These authors explain the smaller intensities by the noise inherent to the ADV, together with the spatial gradients averaging within the sampling volume. Reynolds shear stress happens to be evaluated in the same way by the ADV and the LDA (see figure 17). Dombroski and Crimaldi [2007] mentioned a difference of about 3% in the region far enough from the flume bed. The larger value in our case is to be linked to noise/uncertainties in the measurements more than to a constant shift. The presence of noise that is specific to inherent traits in how the ADV senses the flow, like non-uniform distribution of the seeding particles in the flow, electronic noise, etc., may explain part of the differences observed with the LDA measurements. This question of noise discrepancies has been debated by various authors like Voulgaris and Trowbridge [1998], McLelland and Nicholas [2000], among others. Among different noise sources,

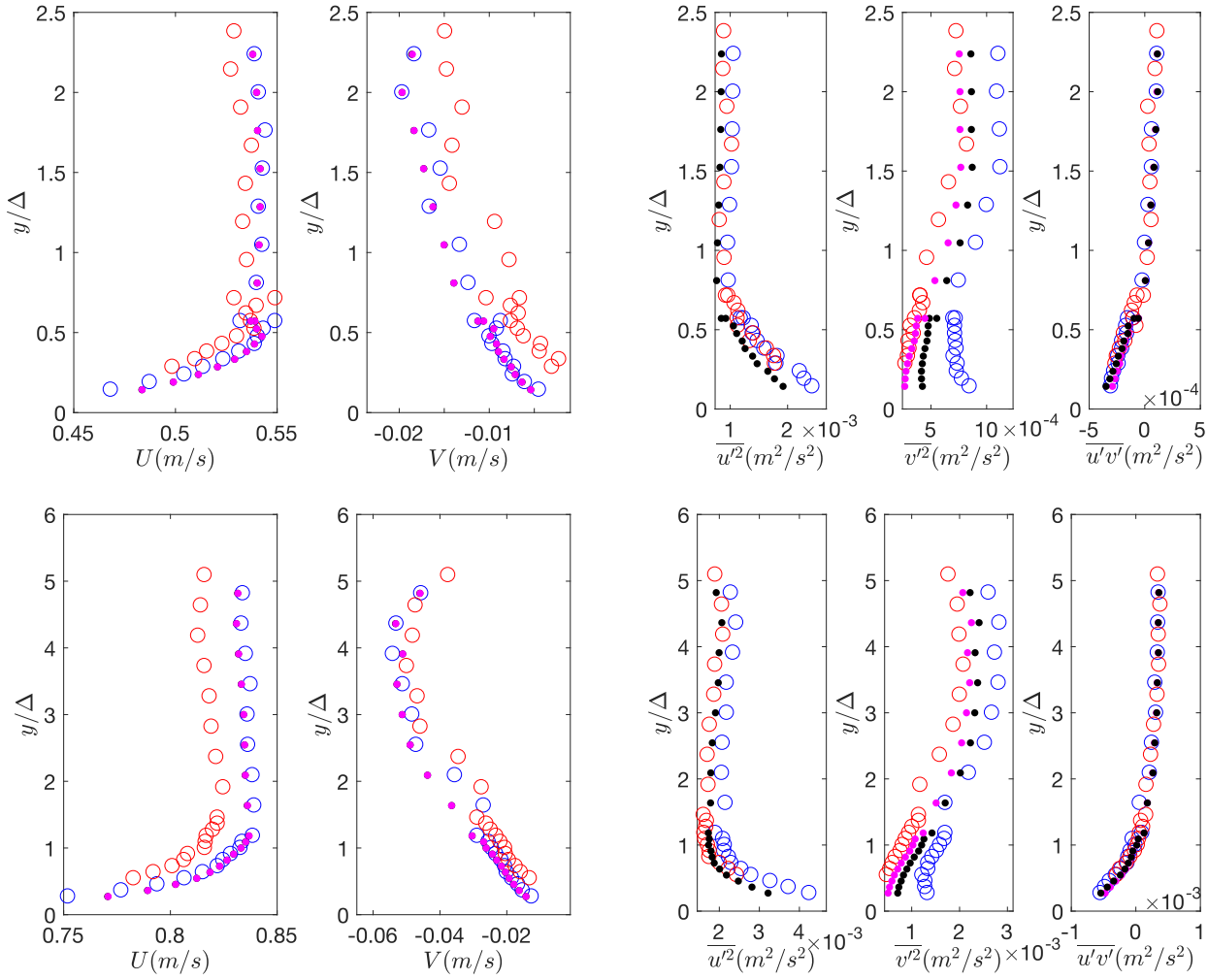

Figure 17: Top: profiles from Exp3, bottom: profiles from Exp5. Quantities measured with ADV (hollow red circle) and LDA (hollow blue circle). From left to right: streamwise mean velocity, vertical mean velocity, fluctuating streamwise intensity, fluctuating vertical intensity, Reynolds shear stress. Filled black point: degraded LDA measurements adapted through the three-step procedure with $N = 2$, filled magenta point: degraded LDA measurements adapted through the three-step procedure with $N = 5$.

no white noise-plateau-like behavior is to be observed in our measurements. If we disregard these tedious questions of noise, the differences between the ADV and the LDA may originate from the sampling rate and the spatial averaging that are respectively lower and larger for the ADV. This appears in the following points:

- The temporal turbulent kinetic energy spectra displayed in Figure 16 indeed confirm that the lower sampling rate of the ADV has some effect. This manifests through a cutoff high-frequency in the spectra that is lower for the ADV than for the LDA. As a consequence, the contribution of the small scales velocities is less well-captured by the ADV than by the LDA measurements, which may explain some of the discrepancies in the turbulent quantities observed between ADV and LDA.
- The second major differences between the ADV and the LDA is that while the LDA is a rather local measuring technique (measuring volume: diameter $D0_{xy} = 0.18$ mm in x- and y-directions, and length $L0_z = 3.87$ mm in the z-direction), the ADV has a measuring volume an order of magnitude larger ($D_{xz} = 6$ mm-diameter in x- and z-directions, and length $L_y \in [2.5mm; 7.6mm]$ in the y-direction). This means that the ADV will tend to spatially average the turbulence and the velocity gradients within this larger measuring volume.
- Concomitantly with the cutoff frequency, the inertial range with the -5/3 slope observed on the temporal spectra is affected. This concerns all the ADV spectra but more specifically those of the vertical velocity component, where the ADV measurements are seen to drop more rapidly from the inertial range.

We explore further in what follows if the ADV-LDA differences we observe could be explained in terms of a mix of sampling and spatial averaging rather than in terms of noise. To do this, we have adopted a heuristic approach. It consists in degrading the LDA data to mimic the ADV behavior, so as to see if such a degradation will reproduce what is measured with the ADV. The approach includes three steps:

1. As pointed out above, the width of the ADV volume in the streamwise direction is much larger than the one of the LDA, namely $D_{xz} = 6$ mm compared to $D_{0xy} = 0.18$ mm. The flow being quasi streamwise ($V \ll U$) implies that the residence time T_{xADV} of a seeding particle inside this volume will be on the order of D_{xz}/U, U being the convection velocity in the x-direction. During T_{xADV}, $N = T_{xADV} \times f_{LDA} = T_{xADV}/T_{LDA}$ velocity samples are validated by the LDA (f_{LDA} and T_{LDA} being the sampling frequency and period of the LDA, respectively). It suggests that the first step for comparing the two metrologies and accounting for this larger residence time of the seeding particles within the ADV sampling volume, is to perform an N points-sliding average on the LDA data, N being determined from f_{LDA} and the convection velocity U (see Figure 18-top).
2. Once the averaging is completed, the second step is the re-sampling of the LDA data at the ADV sampling frequency f_{ADV}. This re-sampling is supposed to account for the weaker temporal resolution of the ADV compared with the LDA.
3. Finally, the height of the ADV volume being subsequent ($L_y \in [2.5mm; 7.6mm]$) it also yields a vertical averaging of the velocities that may influence the measurement accuracy, especially in the flow regions with high local velocity gradients. As the mean velocity gradients remain moderate in the region we explored (outer log-region and beyond), this

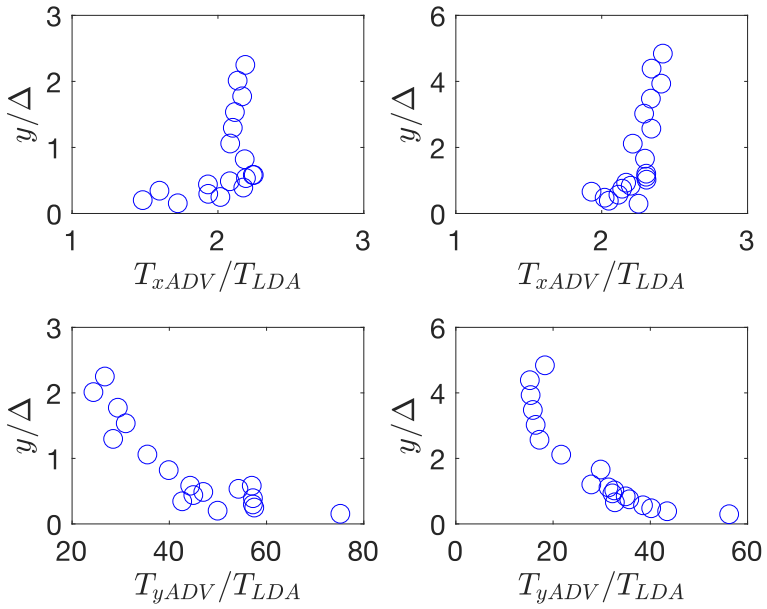

Figure 18: Comparison between characteristic flow times to cross the ADV sampling volume and LDA typical time rate. Top: streamwise direction, Bottom: vertical direction, left: Exp 3, right: Exp5.

vertical averaging should mostly affect the turbulent quantities. Given that $V \ll U$, the characteristic vertical time scale for the flow $T_{yADV} = L_y/V$ are much larger than the typical LDA time scale (T_{LDA}) (see Figure 18-bottom). Hence, the idea is that the vertical ADV averaging effect on the mean and turbulent quantities can be mimicked by averaging the local streamwise and vertical velocities of the LDA profiles over the height falling within the vertical extension of the ADV sampling volume. For example for U this is written as:

$$U_{Nsy}(i) = \frac{1}{L_y} \sum_{i-L_y/2}^{i+L_y/2} U_{Ns}(j) \tag{5}$$

wherein L_y is the volume height given in Table 1 and U_{Ns} is the streamwise mean velocity obtained after steps 1 and 2. V_{Nsy}, $\overline{u'_{Nsy}{}^2}$, $\overline{v'_{Nsy}{}^2}$ and $\overline{u'_{Nsy}v'_{Nsy}}$ are processed in the same way.

In this approach, the only parameter that needs to be specified is the number N of velocity samples validated by the LDA during the streamwise residence time of the seeding particles T_{xADV} within the ADV sampling volume : $N = T_{xADV} \times f_{LDA} = T_{xADV}/T_{LDA}$. We see in Figure 18-top that with $T_{LDA} = 1/f_{LDA}$ estimated from the typical f_{LDA} for each experiment set (Table 1), the order of magnitude of T_{xADV}/T_{LDA} is of a couple units. Taking this order of magnitude for N in the approach yields the results depicted in the plots in Figures 16 and 17. In particular, we see that the temporal turbulent kinetic energy spectra of $\overline{u'_{Nsy}{}^2}$ in Figure 16, obtained by degrading the LDA signal with $N = 2$, behave rather similarly to those of the

ADV at high frequencies. To get the same result for the turbulent energy spectra of $\overline{v'_{Nsy}{}^2}$, a higher value of N ($N = 5$) is needed. This value is strictly speaking larger than the 2-value that appears in figure 18-top but of the same order of magnitude from a heuristic point of view. The consequences of using $N = 2$ and $N = 5$ for calculating the mean and turbulent profiles are shown in Figure 17. Degrading the LDA data reduces significantly the differences existing between the ADV and the LDA on the turbulence intensities. Again, $N = 5$ works better for $\overline{v'}^2$ while $N = 2$ happens to be the right streamwise degrading process for $\overline{u'}^2$. Interestingly, the degrading process proves to have no effect on $\overline{u'v'}$. Perhaps, one of the most important conclusions from these figures is that degrading the LDA data, as we have proposed to mimic the frequency and scale of the ADV measurements has strictly no effect on the detected mean velocities. Indeed, filled black points ($N = 2$) and filled magenta points ($N = 5$) strictly fall on top of each other in figure 17 left (U and V) and within the hollow blue circle of LDA measurements as well. We estimated the spatial averaging effect of our ADV system using the approach proposed by Voulgaris and Trowbridge [1998]. Equation (16) in their work gives the variation of velocity that is averaged by the size of the ADV in the log region. This variation relative to the local velocity is 2-4% higher than that with LDA close to the bed and thus significant. However by approximating the spatial averaging within the sample volume by a linear velocity interpolation, we can show that these velocity variation leads to a relative velocity underestimation only one or two order of magnitude lower than that measured by LDA in Figure 17. This would suggest that the ADV-LDA differences we observe on these mean velocities are more likely linked to a constant bias that the ADV seemingly has or on some ADV-intrinsic noise, rather than to the differences in time and spatial resolutions.

6 Conclusion

This study focused on concurrent ADV and LDA measurements within developing narrow open-channel flows in a laboratory flume. By varying flow discharge, flow depth and inclination, a $Re - Fr$ map was covered ($4 \times 10^4 \leq Re \leq 1.2 \times 10^5$, $0.2 \leq Fr \leq 1.8$). Flow measurements have been carried out in the log-layer and in the outer layer. The LDA-measured turbulence characteristics in the log-layer are found similar to those reported in classical channel flow studies [Gad el Hak and Bandyopadhyay, 1994, Peruzzi et al., 2020]. In contrast, turbulence in the outer layer is high and almost isotropic which flattens the mean streamwise velocity profile in this region. This outer turbulence originates from the three-dimensional energetic flow structures created upstream in the hydraulic circuit and advected in the test section. The Reynolds shear stress becomes negative in the outer region. The location where this happens lies close to the height where the streamwise velocity is maximum and the turbulence becomes isotropic. The use of this height (Δ) where shear stress changes signs to scale the flow collapses the Reynolds shear stress and the mean streamwise deficit velocity profiles remarkably well. It happens to be the effective thickness of the developing boundary layer in the measuring section. It corresponds to the depth where the effects of the free stream turbulence extend into the flow layer developing on the channel bed.

Inserting the ADV into a narrow ($\approx 30\,\mathrm{cm}$) channel flow is found to alter the flow characteristics that the device is intended to measure. When immersing the ADV sensor in the flume, an intrusion effect can be noticed on the detected mean quantities while fluctuating quanti-

ties are not impacted at the measuring position. This has been shown by comparing the LDA measurements obtained at the same location in the flow with and without the ADV sensor immersed. The mean vertical velocity is significantly increased by the presence of the sensor no matter the variation in the value of Fr (up to 200%). On the other hand, the intrusion effect on the streamwise velocity is Fr-dependent. For "low" values ($Fr \leq 0.6$), blocking effects of the ADV contribute to accelerating the streamwise velocity in our narrow flow, while for $Fr > 1.1$ a two-phase wake develops behind the ADV sensor resulting in a slight deceleration of the streamwise velocity (less than 1%). In between ($0.6 \leq Fr \leq 1.1$), the presence of the sensor generates a rise in the elevation of the free surface by up to 10% of the flow depth, which (for most of the time) accelerates the streamwise flow, but in some limited situations causes a slow-down. Some heuristic models have been proposed that are in agreement with the streamwise mean flow experimental results.

The ADV is found to underestimate the key properties of fluid motion compared to the LDA values within a given environment. Comparisons of simultaneous measurements with ADV and LDA at the same location in the flow reveal that the ADV underestimates all the velocity statistics (mean, fluctuating, streamwise, vertical). However, the Reynolds shear stress values are comparable to those measured by the LDA. We have used the LDA data in a heuristic approach to mimic the lower sampling rate that the ADV usually has together with its larger sampling volume to gain insights on how and why the ADV underestimates the flow velocities that it measures. The conclusion is that lower sampling rate and larger sampling volume can explain the differences between the measured turbulence quantities, but not between the mean velocities. It suggests that underestimations of the mean velocities are likely linked to a constant bias of the ADV or to some type of ADV-intrinsic noise.

These findings provide insights into the nature and accuracy of ADV flow measurement when the flow is not necessarily the commonly studied fully developed channel flow. It can be useful for scientists and engineers when interpreting field and laboratory measurements by ADVs in practical situations where the particular flow conditions need to be taken into account such as for example in sediment entrainment and transport, erosive potential, drag forces on structures, and thermal and solute mixing... The value of Fr should be taken into account when interpreting ADV data. In general, mean streamwise flow velocity is likely to be slightly underestimated. However, the net underestimation of the streamwise flow velocity in a low Fr fluid environment likely accounts for the offsetting tendency of the ADV to slightly accelerate the flow when it is introduced into a narrow fluid environment ($b/H \approx 2 - 3$). Additional caution should be taken when evaluating ADV-measured vertical flow and flow fluctuations which are likely to depart more significantly from LDA measurements.

Acknowledgements

We are grateful to Dr. Faouzi Laadhari at LMFA, France and Prof. Jeffrey Koseff at Stanford University, USA for helpful discussions. Prof. Venayagamoorthy gratefully acknowledges the Monfort Professorship through the Monfort Excellence Fund for providing funds for this study.

References

J. Aberle, C. Rennie, D. Admiraal, and M. Muste. Experimental Hydraulics: Methods, Instrumentation, Data Processing and Management: Volume II: Instrumentation and Measurement Techniques. CRC Press, 2017.

P. Buchhave, W.K. George Jr, and J.L. Lumley. The measurement of turbulence with the laser-doppler anemometer. Annu. Rev. Fluid Mech., 11(1):443–503, 1979.

S.M. Cameron, V.I. Nikora, and M.T. Stewart. Very-large-scale motions in rough-bed open-channel flow. J. Fluid Mech., 814:416–429, 2017.

H. Chanson, M. Trevethan, and S.-I. Aoki. Acoustic doppler velocimetry (adv) in small estuary: field experience and signal post-processing. Flow Meas. and Instrum., 19(5):307–313, 2008.

Z. Chara and V. Matousek. Comparative study of adv and lda measuring techniques. In Proceedings of the 6th International Symposium on Ultrasonic Doppler Methods for Fluid Mechanics and Fluid Engineering, 2010.

Y. Chen, B. Lin, J. Lin, and S. Wang. Experimental study of wake structure behind a horizontal axis tidal stream turbine. Appl. Energy, 196:82–96, 2017.

F.H. Clauser. The turbulent boundary layer. In Adv. Appl. Mech., volume 4, pages 1–51. Elsevier, 1956.

D. Coles. The law of the wake in the turbulent boundary layer. J. Fluid Mech., 1:191–226, 1956.

S.K. Delavan, S. Sood, A. Pérez-Fuentetaja, and A.R. Hannes. Anthropogenic turbulence and velocity barriers for upstream swimming fish: a field study on emerald shiners (notropis atherinoides) in the upper niagara river. Ecol. Eng., 101:91–106, 2017.

L. Dey, A.K. Barbhuiya, and P. Biswas. Experimental study on bank erosion and protection using submerged vane placed at an optimum angle in a 180° laboratory channel bend. Geomorphology, 283:32–40, 2017.

E. Dogan, R. E. Hanson, and B. Ganapathisubramani. Interactions of large-scale free-stream turbulence with turbulent boundary layers. J. Fluid Mech., 802:79–107, 2016.

D.E. Dombroski and J.P. Crimaldi. The accuracy of acoustic doppler velocimetry measurements in turbulent boundary layer flows over a smooth bed. Limnol. Oceanogr.-meth., 5(1): 23–33, 2007.

C.M. Finelli, D.D. Hart, and D.M. Fonseca. Evaluating the spatial resolution of an acoustic doppler velocimeter and the consequences for measuring near-bed flows. Limnol. Oceanogr., 44(7):1793–1801, 1999.

M. Gad el Hak and P.R. Bandyopadhyay. Reynolds number effects in wall-bounded turbulent flows. Appl. Mech. Rev., 47(8), 1994.

W.K. George and J.L. Lumley. The laser-doppler velocimeter and its application to the measurement of turbulence. J. Fluid Mech., 60(2):321–362, 1973.

D.G. Goring and V.I. Nikora. Despiking acoustic doppler velocimeter data. J. Hydr. Eng., 128 (1):117–126, 2002.

P.E. Hancock and P. Bradshaw. The effect of free-stream turbulence on turbulent boundary layers. J. Fluids Eng., 105(284), 1983.

P.E. Hancock and P. Bradshaw. Turbulence structure of a boundary layer beneath a turbulent free stream. J. Fluid Mech., 205:45–76, 1989.

N. Hutchins, T.B. Nickels, I. Marusic, and M.S. Chong. Hot-wire spatial resolution issues in wall-bounded turbulence. J. Fluid Mech., 635:103–136, 2009.

Y. Jooss, L. Li, T. Bracchi, and R.J. Hearst. Spatial development of a turbulent boundary layer subjected to freestream turbulence. J. Fluid Mech., 911:A4–1–A4–27, 2021.

B. Khorsandi, L. Mydlarski, and S. Gaskin. Noise in turbulence measurements using acoustic doppler velocimetry. J. Hydr. Eng., 138(10):829–838, 2012.

M.S. Kirkgöz and M. Ardiçlioğlu. Velocity profiles of developing and developed open channel flow. J. Hydraul. Engng, 123(12):1099–1105, 1997.

B.A. Kironoto and W. Graf. Turbulence characteristics in rough non-uniform open-channel flow. In In Proc., Instn. Civ. Engrs. Water, Maritime, and Energy, volume 112, pages 336–348, 1998.

A. Lohrmann, R. Cabrera, and N.C. Kraus. Acoustic-doppler velocimeter (adv) for laboratory use. In Fundamentals and advancements in hydraulic measurements and experimentation, pages 351–365. ASCE, 1994.

A. Lohrmann, R. Cabrera, G. Gelfenbaum, and J. Haines. Direct measurements of reynolds stress with an acoustic doppler velocimeter. In Proceedings of the IEEE Fifth Working Conference on Current Measurement, pages 205–210. IEEE, 1995.

C. A. Martin and T. K. Gates. Uncertainty of canal seepage losses estimated using flowing water balance with acoustic doppler devices. J. Hydrol., 517:746–761, 2014.

S.J. McLelland and A.P. Nicholas. A new method for evaluating errors in high-frequency adv measurements. Hydrol. process., 14(2):351–366, 2000.

G.L. Mellor and D.M. Gibson. Equilibrium turbulent boundary layers. J. Fluid Mech., 24: 225–253, 1966.

M. Muste, D. Lyn, D. Admiraal, R. Ettema, V. Nikora, and M.H. García. Experimental Hydraulics: Methods, Instrumentation, Data Processing and Management: Volume I: Fundamentals and Methods. CRC Press, 2017.

I. Nezu and H. Nakagawa. Turbulence in Open Channel Flows. Balkema, The Netherlands, 1993.

C. Peruzzi, D. Poggi, L. Ridolfi, and C. Manes. On the scaling of large-scale structures in smooth-bed turbulent open-channel flows. J. Fluid Mech., 889, 2020.

C.M. Poindexter, P.J. Rusello, and E.A. Variano. Acoustic doppler velocimeter-induced acoustic streaming and its implications for measurement. Exp. Fluids, 50(5):1429–1442, 2011.

E. Precht, F. Janssen, and M. Huettel. Near-bottom performance of the acoustic doppler velocimeter (adv)–a comparative study. Aquat. Ecol., 40(4):481–492, 2006.

A.L. Quaresma, R.M.L. Ferreira, and A.N. Pinheiro. Comparative analysis of particle image velocimetry and acoustic doppler velocimetry in relation to a pool-type fishway flow. J.Hydr. Res., 55(4):582–591, 2017.

M. Romagnoli, C.M. García, and R.A. Lopardo. Signal postprocessing technique and uncertainty analysis of adv turbulence measurements on free hydraulic jumps. J. Hydr. Eng., 138 (4):353–357, 2012.

V. Roussinova, N. Biswas, and R. Balachandar. Revisiting turbulence in smooth uniform open channel flow. J. Hydr. Res., 46(sup1):36–48, 2008.

P.J. Rusello, A. Lohrmann, E. Siegel, and T. Maddux. Improvements in acoustic doppler velocimetry. In Proc. of the 7^{th} Int. Conf. on Hydro. and Eng. Michael Piasecki and College of Engineering, Drexel University, 2006.

S. Sarkar. Measurement of turbulent flow in a narrow open channel. J. Hydrol. and Hydromech., 64(3):273–280, 2016.

N. S. Sharp, S. Neuscamman, and Z. Warhaft. Effects of large-scale free stream turbulence on a turbulent boundary layer. Phys. of Fluids, 21(095105), 2009.

A. M. Shinneeb, G. Nasif, and R. Balachandar. Effect of the aspect ratio on the velocity field of a straight open-channel flow. Phys. of Fluids, 33(085110), 2021.

C. Tropea and A.L. Yarin. Springer handbook of experimental fluid mechanics. Springer Science & Business Media, 2007.

G. Voulgaris and J.H. Trowbridge. Evaluation of the acoustic doppler velocimeter (adv) for turbulence measurements. J. Atmos. Ocean. Technol., 15(1):272–289, 1998.

T. Wei, R. Schmidt, and P. McMurtry. Comment on the clauser chart method for determining the friction velocity. Exp. Fluids, 38(5):695–699, 2005.